PCCP

PAPER

View Article Online
View Journal | View Issue

Cite this: *Phys. Chem. Chem. Phys.*, 2015, **17**, 6644

Möbius–Hückel topology switching in an expanded porphyrin cation radical as studied by EPR and ENDOR spectroscopy†

Klaus Möbius,*[ab] Martin Plato,[a] Gudrun Klihm,[b] Christoph Laurich,[b] Anton Savitsky,*[b] Wolfgang Lubitz,[b] Bartosz Szyszko,[c] Marcin Stępień[c] and Lechosław Latos-Grażyński*[c]

Received 9th December 2014,
Accepted 3rd February 2015

DOI: 10.1039/c4cp05745g

www.rsc.org/pccp

The symmetry of the arrangement of objects has fascinated philosophers, artists and scientists for a long time, and still does. Symmetries often exist in nature, but are also created artificially, for instance by chemical synthesis of novel molecules and materials. The one-sided, non-orientable Möbius band topology is a paradigm of such a symmetry-based fascination. In the early 1960s, in synthetic organic chemistry the interest in molecules with Möbius symmetry was greatly stimulated by a short paper by Edgar Heilbronner. He predicted that sufficiently large [*n*]annulenes with a closed-shell electron configuration of 4*n* π-electrons should allow for sufficient π-overlap stabilization to be synthesizable by twisting them with a 180° phase change into the Möbius symmetry of their hydrocarbon skeleton. In 2007, the group of Lechosław Latos-Grażyński succeeded in synthesizing the compound di-*p*-benzi[28]hexa-phyrin(1.1.1.1.1.1), compound **1**, which can dynamically switch between Hückel and Möbius conjugation depending, in a complex manner, on the polarity and temperature of the surrounding solvent. This discovery of "topology switching" between the two-sided (Hückel) and one-sided (Möbius) molecular state with closed-shell electronic configuration was based primarily on the results of NMR spectroscopy and DFT calculations. The present EPR and ENDOR work on the radical cation state of compound **1** is the first study of a ground-state open-shell system which exhibits a Hückel–Möbius topology switch that is controlled by temperature, like in the case of the closed-shell precursor. The unpaired electron interacting with magnetic nuclei in the molecule is used as a sensitive probe for the electronic structure and its symmetry properties. For a Hückel conformer with its higher symmetry, we expect – and observe – fewer ENDOR lines than for a Möbius conformer. The ENDOR results are supplemented by and in accordance with theoretical calculations based on density functional theory at the ORCA level.

1. Introduction

The Möbius band has been an object of fascination both in the arts and sciences, and much has been written about such lines of thought and inspiration.[1–13] In organic chemistry the interest in molecules with Möbius topology was stimulated by a paper by Edgar Heilbronner[8] in which he predicted, on the basis of Hückel molecular orbital (HMO) theory,[14–16] that sufficiently large molecules of annulenes should be capable of reaching adequate π-overlap in a twisted Möbius-band configuration. Hence, Heilbronner's prediction extended the Hückel rule by disclosing a complementary type of aromaticity, wherein Möbius systems with [4*n*] π-electrons are "Möbius aromatic", whereas those with [4*n* + 2] π-electrons are "Möbius antiaromatic". The premise for this to happen is the easy accessibility of non-planar conformations, *i.e.*, the annulene molecules must be large enough to avoid too much steric strain that would not be overcompensated by additional π-conjugation.[8,17] The concept of Möbius topology as a determining factor for aromaticity in organic molecules has gained further momentum from quantum chemistry theory with large-scale calculations up to the level of modern density functional theory (DFT).[18–22] A number of theoretical and experimental papers followed.[3,4,9,10,20,23,24]

Quite a number of organic chemistry laboratories took on the challenge to synthesize Möbius-type conjugated molecules.

[a] *Freie Universität Berlin, Fachbereich Physik, Arnimallee 14, 14195 Berlin, Germany. E-mail: moebius@physik.fu-berlin.de*
[b] *Max Planck Institut für Chemische Energiekonversion, Stiftstr. 34-36, 45470 Mülheim (Ruhr), Germany. E-mail: anton.savitsky@cec.mpg.de*
[c] *Wydział Chemii, Uniwersytet Wrocławski, ul. F. Joliot-Curie 14, 50-383 Wrocław, Poland. E-mail: lechoslaw.latosgrazynski@chem.uni.wroc.pl*

† Electronic supplementary information (ESI) available: Details of the DFT calculations of ^{14}N- and ^{1}H hyperfine couplings of the cation radicals of the Möbius and Hückel conformers. See DOI: 10.1039/c4cp05745g

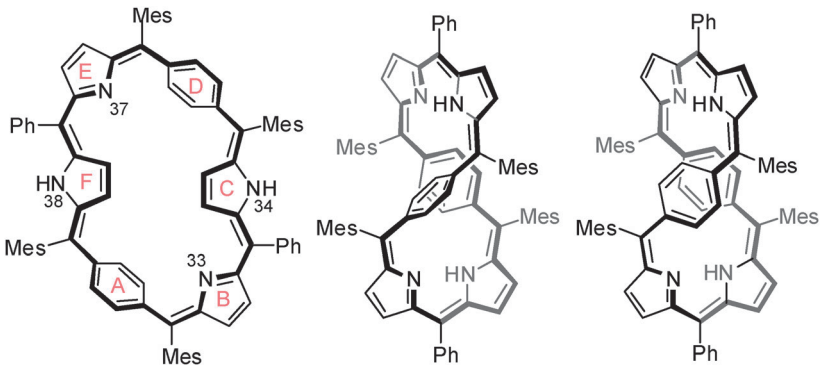

Scheme 1 Accessible conformations of free-base **1** (Mes = mesityl, Ph = phenyl). The 28-π-electron conjugation pathway is shown in bold. The cation radical of form *T0*-**1** was not observed in the present EPR study.

But it was not until 2003 when the first synthesis of an aromatic Möbius annulene was accomplished by Rainer Herges and co-workers.[25,26] Subsequently, it has been demonstrated that expanded porphyrinoids can acquire Möbius topologies.[9,12,20,24,27–49] In this group of compounds several different approaches have been applied to induce Möbius-strip structures including protonation,[12,36] metal and metalloid coordination,[29,32,39,40,43] and fusion reactions.[34,38,41]

In 2007, the Wrocław group of Lechosław Latos-Grażyński succeeded to synthesize the compound di-*p*-benzi[28]hexaphyrin-(1.1.1.1.1.1), **1** (Scheme 1), which can dynamically switch between Hückel and Möbius aromaticity depending on the polarity and temperature of the surrounding solvent.[20] Di-*p*-benzihexaphyrin **1** combines structural features of expanded porphyrins[10,24,44,46,50] and benziporphyrins.[27,28,51–55]

The macrocyclic framework is built of four pyrrolic (B, C, E, F, Scheme 1) and two *p*-phenylene rings (A and D). It is the relative arrangement of these two benzene rings, acting as "topology selector", that allows the molecule to switch between twisted Hückel (*T2*-**1**) and Möbius (*T1*-**1**) topology without any covalent bonds being broken. In the figure-of-eight conformation, the two benzene rings can form a parallel setting (twisted Hückel antiaromatic, *T2*-**1**), or orient themselves to each other perpendicularly (Möbius aromatic, *T1*-**1**).[9,10,20] Room-temperature solutions of **1** dissolved in chlorinated solvents contain an equilibrium mixture of *T1* and *T2* conformers. Lowering the temperature of solution shifts the equilibrium towards Möbius aromatic structure, while raising the temperature favours the Hückel antiaromatic species. The Hückel species is also the dominant form of **1** when dissolved in aliphatic hydrocarbons and alcohols. In addition to *T1* and *T2* conformers, a planar Hückel metastable form *T0* was also observed by Stępień *et al.*[9,10] during the deprotonation of hexaphyrin **1** dications at low temperatures.

The present work is the first study of a ground-state open-shell system which exhibits a Hückel–Möbius topology switch, like the closed-shell precursor does. It should be emphasized here that up to now only ground-state closed-shell Möbius systems have been studied both theoretically and experimentally.

For an open-shell system, the appropriate spectroscopic tool for characterizing such switchable topologies in detail is EPR spectroscopy and its extension to electron-nuclear double resonance (ENDOR). The unpaired electron interacting with magnetic nuclei ($I \neq 0$) in the molecule (hyperfine interaction) is used as a sensitive probe for the electronic structure and symmetry properties of the open-shell system.[56] Such symmetry aspects are particularly important in ENDOR since this method essentially allows one to identify the topology of the observed species by merely counting the number of lines in the ENDOR spectrum, because this number is determined by the symmetry of the molecule. Thus, for a Hückel structure with its higher symmetry, we expect fewer ENDOR lines than for a Möbius conformer. The ENDOR experiments are supplemented by theoretical calculations based on density functional theory.

Our main motivation in pursuing this work is to examine whether a Hückel–Möbius topology switch in an expanded porphyrin **1** exists not only in its singlet ground state[9,10] but also in its radical doublet groundstate. The switch can be controlled by a proper choice of solvent, temperature and counter-ion. The present report is restricted to radical cations of **1**, but work is in progress also on radical anions of **1**.

2. Experimental

5,15,20,30-Tetramesityl-10,25-diphenyl-*A*,*D*-di-*p*-benzihexaphyrin-(1.1.1.1.1.1), compound **1**, was synthesized as described earlier.[20,27,28] The yield of the synthesis of *A*,*D*-di-*p*-benzi-[28]hexaphyrin(1.1.1.1.1.1), starting from pyrrole, is extremely low (*ca.* 5%). This renders isotope labeling by ^{15}N practically inaccessible, although this would be desirable as far as ENDOR spectroscopy is concerned.

Liquid-solution cw (continuous wave) EPR and ENDOR spectra of the radical cations of **1** were recorded in three different solvents: dichloromethane (CH_2Cl_2), chloroform ($CHCl_3$) and dimethylformamide (DMF), over a temperature range between 190 K and 330 K. This wide temperature range was chosen to get the largest possible population differences between the two conformers, the Möbius form *T1*-**1** (dominant at low temperatures) and the Hückel form *T2*-**1** (dominant at high temperatures). The caveat of this approach is that at 190 K both $CHCl_3$ and DMF are close

to their melting points (210 K and 212 K, respectively, for the pure solvents). On the other hand, CH_2Cl_2 has a sufficiently low melting point (177 K) to cause no problem in this respect. However, the highest temperature (330 K) slightly exceeds the boiling point (313 K) of pure CH_2Cl_2 at normal pressure, but, due to the sealed sample tubes, the liquid phase was always retained, as was apparent from observing the quality factor of the microwave cavity. There is another reason for preferring CH_2Cl_2 over the other two solvents: since the switching behavior between Hückel and Möbius aromaticity depends, among other parameters, on the polarity of the surrounding solvent,[20] $CHCl_3$ is an unfavourable solvent also because of its considerably lower polarity ($\varepsilon(CH_2Cl_2) = 9.1$, $\varepsilon(CHCl_3) = 4.9$). Although DMF has an even higher polarity than CH_2Cl_2, (ε(DMF) = 38.3), all our ENDOR measurements for this solvent in the accessible low (Möbius) or high (Hückel) temperature regions resulted in spectra with very poor S/N ratio. Apparently, the critical requirements for the ENDOR-in-solution effect in terms of viscosity and temperature cannot be matched for this radical–solvent system.[56] Consequently, we focus the following discussion on the ENDOR results obtained for the solvent CH_2Cl_2. The ENDOR measurements were performed in different rf frequency ranges, *i.e.*, between 12 MHz and 17 MHz for the detection of ^{1}H resonances and between 0 MHz and 8 MHz for ^{14}N resonances. Experimental parameters, such as radical concentration as well as mw and rf power, were varied to optimize the cw ENDOR signal-to-noise ratio.

The radical cations of **1** in CH_2Cl_2 were generated coulometrically under controlled potential at room temperature using a potentiostat EG&G 283. The coulometry was performed under high-vacuum conditions in a home-built electrolysis cell using tetrabutylammonium hexafluorophosphate ($TBAPF_6$) as supporting electrolyte. The coulometry setup with four electrodes was connected to a high-vacuum line to ensure oxygen-free conditions. The reference electrode was made from an uncoated silver wire. The second electrode was a platinum wire, the third one a platinum net, and the fourth one was the counter electrode. Compound **1** (1 mM) and supporting electrolyte $TBAPF_6$ (10 mM) were put into the cell and degassed by high-vacuum pumping. About 1 mL of CH_2Cl_2 (dried over CaH_2 and deoxygenated using three freeze–pump–thaw cycles) was then distilled into the electrolysis cell from the high-vacuum line with its detachable solvent flask.

Cyclic voltammetry of compound **1** was measured before performing coulometry to assure reversibility of the one-electron oxidation reaction, and to check for the correct redox potential of the sample. In the cyclic voltammetry measurements the Pt-wire acted as working electrode, whereas for the coulometric radical-sample generation, the Pt-net was used as a working electrode. The applied voltage was 100 mV more positive than the first oxidation peak. Oxidation was performed using a charge quantity of 85 mC which, under ideal conditions, yields 85% singly oxidized compound **1**. The estimated radical-ion concentration was about 10^{-3} M. An EPR pyrex sample tube (3 mm o.d.; 2 mm i.d.) was directly fused to the coulometry cell. About 40–100 μL of the solution were transferred to the EPR sample tube and frozen in liquid nitrogen. Subsequently, the tube was pumped, flame sealed and inserted into the ENDOR cavity containing the Dewar for sample temperature control.

Cw EPR and ENDOR measurements at X-band microwave (mw) frequency (9.5 GHz) were performed with a computer-controlled ER 200D spectrometer (Bruker) upgraded with home-built ENDOR and TRIPLE resonance accessories.[57] For optimizing the ENDOR detection sensitivity, a new TM_{110}-type mw cavity/ENDOR coil arrangement was constructed[58] which is based on design principles described earlier.[59,60] The advantages of this cavity are stable mw coupling and constant mw field B_1 over the sample volume, a high Q factor ($\approx$5000) and high radio-frequency (rf) NMR field B_2 available over a wide rf frequency range to cover nitrogen and proton NMR transition frequencies (up to 2 mT (rotating frame) at 14 MHz for ^{1}H ENDOR and 3 mT (rotating frame) at 2 MHz for ^{14}N ENDOR). The rf power can be leveled in such a way to achieve a constant effective B_2 field across the whole ENDOR spectrum. The temperature at the sample could be adjusted between 100 K and 350 K, using a temperature-control system with nitrogen gas passing through a quartz Dewar that is placed inside the ENDOR cavity. For the analysis of the ENDOR patterns a simulation program was used which has been developed in our laboratory.

3. Theoretical

The observed line splittings in the ENDOR spectra of the radical cations of **1** in liquid solutions are caused by the isotropic hyperfine interactions of the delocalized unpaired electron with the various nuclei n of the molecular skeleton. Quantitatively, this "Fermi contact" interaction is described by the scalar hyperfine coupling constant (hfc) a_n. Its value is proportional to the squared amplitude of the electronic wave function at the associated nucleus n, *e.g.*, n = ^{14}N or ^{1}H.[61] It can be calculated by the nowadays widely accepted quantum chemical density functional method DFT.[62,63] This method is an essential component of the software package ORCA (Version 3.0) developed by Frank Neese and coworkers.[64]

For a set of a_n values, the ENDOR line positions on the frequency scale are given by

$$\nu_{ENDOR} = |\nu_n \pm a_n/2| \quad (1)$$

expressing the fact that two lines, symmetrically placed around the free nuclear Larmor frequency $|\nu_n|$ or $|a_n/2|$, whichever is larger, are expected for each set of symmetry-equivalent nuclei n with an hfc a_n.

Nuclear coordinates are adopted from the publication of Stępień and coworkers.[9] Their listings contain the Cartesian coordinates for the DFT-optimized structures of both the Möbius (*T1*-**1**) and Hückel (*T2*-**1**) molecules in their neutral singlet ground states. These structures were obtained by minimum-energy geometry optimization with the functional B3LYP[62,63] and basis set 6-31G**[65] on predetermined single-crystal X-ray structures. They comprise altogether 158 atoms (82 C, 72 H, 4 N), resulting in 420 or 419 valence electrons in the neutral singlet ground state or cation doublet state, respectively.

Other essential DFT program settings concern the choice of a closed or open shell treatment, of a geometry optimization

run and of various accuracy options. We have taken various refinement approaches defined as Cases 1 to 7 and specified in Tables S1 and S2 of the ESI.† For these refinements the isotropic hfc's belonging to the four ^{14}N- and selected ^{1}H-positions in both structures, *T1*-**1** and *T2*-**1**, were calculated. Additional calculations have been performed to acquire the total energies of the two conformers and, thereby, to determine their relative stability. They include the use of the basis set Def2-TZVP (TZVP = triple zeta valence basis set including f-polarization functions).[66] This basis set is particularly well-suited for determining molecular wave functions in the near vicinity of nuclei in organic systems. However, this quite elaborate basis set requires CPU times at least 10 times longer than conventional double-zeta Pople-type basis sets, *e.g.*, 6-31G**.

Another important feature of ORCA is the implementation of the COSMO solvation model developed by Klamt and Schüürmann.[67] This model describes the solvent as a dielectric polarizable continuum. It is initially assumed to be a perfect conductor which completely shields the charge density of the solute. The interaction is then scaled to a finite dielectric constant by an empirical relation. COSMO works as an iterative process in order to find self-consistent values of the screening charges and the molecular charge density.

All calculations were performed on the HERMES cluster at the Max Planck Institute for Chemical Energy Conversion in Mülheim (Ruhr) with 65 nodes each having 12 cores and 48 GB RAM.

4. Results and discussion

4.1 Experimental

The EPR spectra of the cation radicals of *T1*-**1** and *T2*-**1** show the broad Gaussian lines typical of unresolved hyperfine structure (see insets of Fig. 1a and b). This is mainly due to inhomogeneous line broadening caused by the large number of magnetically inequivalent protons in the molecule. Hence, the EPR spectra lost most of their structural information and are indistinguishable for the *T1*-**1** and *T2*-**1** conformations. Therefore, we resort to ENDOR with its inherently higher resolving power. But, even the ^{1}H-ENDOR spectra are characterized by a large number of lines (>70), which overlap in the narrow frequency range between 12 MHz and 17 MHz and, hence, are exceedingly difficult to disentangle. Thus, the present analysis concentrates on the ^{14}N spectra for which a maximum of eight lines is expected for symmetry reasons. Our preferential choice of the solvent CH_2Cl_2 is even more justified because of the fact that here the topological switching between the Möbius and Hückel topologies was most convincingly observed in our experiments (see Fig. 1). It should be pointed out that, owing to the complexity of the electronic structure of compound **1** and its changes under solvent and temperature variation, the ENDOR-determined hyperfine couplings alone do not allow one to identify the Hückel–Möbius topology switch, but need to be unambiguously assigned and analyzed by advanced quantum chemical calculations (here at the DFT level).

^{14}N-ENDOR spectra. Since the proton ENDOR spectra are characterized by a large number of close-lying lines, most of which are exceedingly difficult to disentangle, we focus mainly on the nitrogen ENDOR spectra (see Fig. 1). According to eqn (1), the ^{14}N-ENDOR spectra are expected to contain at most eight separated lines from the four nitrogens over the frequency range 0 MHz to 4.5 MHz. From the observed line positions, we derived the corresponding ^{14}N-ENDOR isotropic hfc's given in Table 1 for both topologies. These results are supported by corresponding spectra simulations also shown in Fig. 1a and b, respectively. Information on the linewidths required for these simulations is included in Table 1.

Both ENDOR spectra in Fig. 1a and b have been corrected for base line drifts after applying low-pass filtering. Spectral ranges below 1.0 MHz are omitted because of instrumentally conditioned

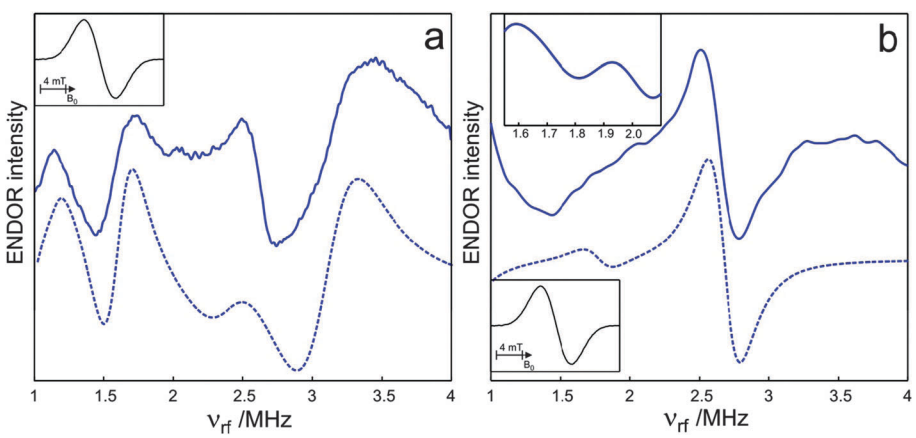

Fig. 1 The liquid-solution ^{14}N cw ENDOR spectra (full lines) of the cation radicals of the conformers *T1*-**1** at 230 K (a) and *T2*-**1** at 330 K (b) in CH_2Cl_2. The ENDOR spectra are shown in the usual first-derivative representation with respect to the rf frequency, ν_{rf}. The simulated ENDOR spectra (dotted lines) of the cation radicals of *T1*-**1** and *T2*-**1** are also shown. The simulations are based on the theoretical ^{14}N hyperfine couplings, a_N^{th}, calculated by ORCA-DFT as guideline. For details, see text and Table 1. The inset in the upper left corner of (b) shows the zoomed frequency section around 1.8 MHz. In the other insets (a, left upper corner, b left lower corner) the cw EPR spectra of the cation radicals of compound **1** at the respective temperatures are shown in the usual first-derivative representation with respect to the external field, B_0.

Table 1 Experimental results for isotropic ^{14}N- and ^{1}H-hyperfine coupling constants with additional information on observed ENDOR line positions and linewidths

	Structure					
	T1-**1**			*T2*-**1**		
Nucleus	Hfc[a]	Position	Linewidth	Hfc	Position	Linewidth
N_{34}(H)	2.70	2.40; 0.30[b]	0.35[c]	3.30[a]	2.70; 0.60[b]	0.20[c]
N_{38}(H)	1.10	1.60; 0.50	0.20	3.30	2.70; 0.60	0.20
N_{33}	4.10	3.10; 1.00	0.40	1.44	1.77; 0.35	0.20
N_{37}	0.20	1.15; 0.95	0.10	1.44	1.77; 0.35	0.20
H(N_{34},N_{38})	3.60	16.4; 12.8	0.10	3.60	16.4; 12.8	0.10

[a] Hyperfine coupling constants in MHz, assignments according to theoretical predictions (see Tables 2 and 3). [b] ENDOR line positions according to eqn (1), in MHz. Free nuclear frequencies: 1.05(^{14}N), 14.6(^{1}H) MHz. [c] Linewidths (half width at half height, Lorentzian line shape), in MHz.

strong noise increase. The simulated ENDOR spectra are based on the theoretical ^{14}N hyperfine couplings, a_N^{th}, which were calculated by ORCA-DFT as guideline. The ENDOR spectrum of *T2*-**1** reveals a resonance feature of relatively low amplitude centered around 1.8 MHz (see upper inset in Fig. 1b). By applying a well-established combination of numerical spectral smoothing and differentiation methods[68] in the ENDOR data analysis across the ν_{rf}-frequency region $1.5 < \nu_{rf} < 2.1$ MHz, this feature could be clearly identified as an additional resonance line. The comparatively low amplitude of this line results from its smaller hyperfine-enhancement factor and smaller nuclear spin–lattice relaxation rate W_n (ref. 56) as compared to the corresponding values for the strong line at 2.70 MHz. For the same reasons, ^{14}N-ENDOR-lines often show a marked decrease in signal amplitude towards lower frequencies.[69] A comparison with the ENDOR lines of ^{15}N labeled compound **1** would have been desirable but was precluded for reasons given above (see Experimental).

In principle, the observed temperature dependence of the ENDOR spectra of the radical cations of **1** point to a two-site exchange process between conformers. Their electronic structures can basically be affected by three mechanisms: (i) by Coulomb interactions because of ion pairing of the radical cations and hexafluorophosphate counter anions, PF_6^-, of the supporting electrolyte, $TBAPF_6$; (ii) by solvation effects of the radical cations; (iii) by different topologies of the cations, or by a combination thereof. If ion pairing would play a substantial role, one would expect that at high temperatures, where the solvent polarity decreases because of averaging-out of the orientational part of the solvent polarization, the electron spin and charge densities of the radical cations get more localized. This would lead to a lower symmetry of the molecular electronic structure.[70] This is in contrast to the experimental ENDOR results which clearly show that at high temperatures the Hückel-conjugated conformer with its higher symmetry dominates, whereas at low temperatures the Möbius-conformer with its lower symmetry dominates. Hence, we conclude that ion pairing is not likely to play a substantial role in the two-site exchange process between the conformers of **1**. We are thus left with mechanisms (ii) and/or (iii) as potential sources for the observed temperature dependence of the ENDOR spectra – analogous to the situation of the neutral singlet-state of **1**. There, the NMR spectra and DFT calculations were interpreted to reflect the topology switching from Hückel to Möbius conformers when lowering the temperature.[9,20]

On physical grounds, we expect different energy gaps ΔH between the radical cations of the two conformers *T1*-**1** and *T2*-**1** than between the corresponding neutral species. In consequence, the equilibrium constants $K = [T2\text{-}\mathbf{1}]/[T1\text{-}\mathbf{1}]$ at different temperatures may also be different for the radical cations and the neutral species. On the other hand, our ENDOR observations on the radical cations show qualitatively the same temperature behavior as found for the neutral states[9,20] in that we also get fairly pure conformers at the temperature limits 230 and 330 K. Even more so, the ENDOR results imply an exceedingly higher concentration (approx. 10 : 1) of *T2*-**1** cations at 330 K relative to that of *T1*-**1** cations. For the neutral species, this ratio is 1.1 : 1, as calculated from the ΔH and ΔS values given in ref. 20. At 230 K, the concentration ratio of *T1*-**1** over *T2*-**1** is found to be approx. 5 : 1 (19 : 1 for the neutral species, ref. 20). Thus, the corresponding relative populations p_H/p_M (H = Hückel, M = Möbius), are estimated as 10.0 at 330 K and 0.2 at 230 K. The given concentration ratios for the cation radicals were determined by simulation of the two respective ENDOR spectra when superimposing different contributions of *T1*-**1** and *T2*-**1**. In the simulation procedure the main additional contribution in Fig. 1a is expected from the line at 2.7 MHz in Fig. 1b. In Fig. 1b, it is mainly the line at 3.2 MHz in Fig. 1a which would cause the strongest changes in the spectral features.

We now estimate the thermodynamic parameters for the two-jump conversion of the *T1*-**1** and *T2*-**1** radical cations. In terms of the associated equilibrium constant $K(T)$, defined by the relative populations p_H/p_M we obtain from the values derived above

$$K(230\ \mathrm{K}) \approx 0.2,\ K(330\ \mathrm{K}) \approx 10.0. \quad (2)$$

Inserting these values into the van't Hoff equation[9]

$$K(T) = \exp(\Delta S/R - \Delta H/RT), \quad (3)$$

where $R = 8.314\ \mathrm{J\ mol^{-1}\ K^{-1}}$ is the universal gas constant and ΔS and ΔH are the reaction entropy and enthalpy changes, yields

$$\Delta H = 25\ \mathrm{kJ\ mol^{-1}},\quad \Delta S = 95\ \mathrm{J\ mol^{-1}\ K^{-1}}. \quad (4)$$

These values for the conversion of the cation radical species are of the same order of magnitude as those found for the neutral singlet-state species[20] (19 kJ mol^{-1}, 59 J mol^{-1} K^{-1} measured in $CDCl_3$). Provided that the solvent effect on the thermodynamic parameters is of minor importance, the larger value of ΔH for the charged species would appear plausible on account of the larger changes in the charge distributions in *T1*-**1** and *T2*-**1** under the site conversion.

The experimental results for the isotropic ^{14}N- and ^{1}H-hyperfine coupling constants are collected in Table 1 together with additional information on the observed ENDOR line positions and widths.

Considerable linewidth variations are observed in particular in the *T1*-**1** spectrum, which is taken at low temperature. This behaviour is typical of an ENDOR spectrum of a radical in

solution in the ''slow-motion regime'', where the rotational motion in the solvent is already considerably slowed down. In this situation, contributions of anisotropic hyperfine interactions to the linewidth become increasingly effective.[71] In the fast rotational motion region at high temperatures, where the *T2*-**1** spectrum is taken, such anisotropic interactions are averaged out, resulting in a practically constant linewidth over the entire spectrum. On the other hand, our results indicate the presence of additional line broadening effects in the *T2*-**1** spectrum as compared to the narrowest lines in the *T1*-**1** spectrum. This is attributed to an increasing influence of Heisenberg exchange[71] towards higher temperatures.

^{1}H-ENDOR spectra. A rather problematic situation is encountered in the case of the proton-ENDOR spectra which, although satisfactory in their signal-to-noise ratio, are difficult to analyze on account of their large number of overlapping lines.

The ^{1}H-ENDOR spectra reveal only one well-resolved hyperfine coupling of 3.6 MHz derived from the two lines symmetrically placed around the free-proton Larmor frequency at 14.6 MHz (see Fig. 2 and Table 1). These lines are sufficiently separated from the otherwise badly resolved accumulation of lines in the central part of the spectrum. We assign this exceptionally large proton hfc to the two protons attached to one pair of the four nitrogen atoms, N_{34} and N_{38} in compound **1**. At present it is unclear why this hyperfine line does not appear at least partly resolved into two different hfc's in the *T1*-**1** spectra, as is predicted by DFT theory (predicted splitting $\Delta\nu \approx 0.4$ MHz, see Case 3 in Table 3). Most probably, the explanation is that a number of energetically close-lying tautomers can coexist at comparable concentration. This would result in an average value of these proton couplings as is the case of the Hückel structure *T2*-**1**.

4.2 Theoretical

All results of the DFT calculations of isotropic hfc's, a_N^{th}, are compiled in tabular form for up to seven different ORCA program settings, including solvent effects by the COSMO model. These tables are contained in the ESI.† The hfc's for ^{14}N nuclei, a_N^{th}, are listed in Table S1 (ESI†), those for ^{1}H nuclei, a_H^{th}, in Table S2 (ESI†). It turns out that the COSMO model calculations yield unsatisfactory results concerning the energetic ordering of the two conformers, *T1*-**1** and *T2*-**1**. This is not unexpected owing to the subtle interplay of the interactions of the solvent molecules with the radical cations and with the counter anions (we thank the referee for pointing this out).

Here, in the main text, we restrict ourselves to Cases 3 and 5, which give the best agreement with the experimental results (see Tables 2 and 3).

The pattern of the selected N and H isotropic hfc's in the radical cations of *T1*-**1** and *T2*-**1**, as determined by DFT calculations (Case 1), is visualized in Fig. 3.

Essential features of the theoretical results are the following: they reflect the increase of molecular symmetry when switching from the Möbius to the Hückel structure, in that both nitrogen

Table 2 ORCA-DFT results for isotropic ^{14}N hyperfine coupling constants a_N^{th} in cation radicals of *T1*-**1** (Möbius) and *T2*-**1** (Hückel), respectively

		a_N^{th}/MHz			
Case[a]	Structure[b]	N_{34}	N_{38}	N_{33}	N_{37}
3[c]	*T1*-**1**	2.64	3.01	4.62	−0.17
	T2-**1**	3.25	3.26	1.44	1.45[e]
5[d]	*T1*-**1**	1.72	3.36	4.10	0.50

[a] Different program settings (functional, basis-set, *etc.*). [b] Initial geometries from optimized X-ray structures.[20] [c] B3LYP,[72] Def2-TZVP.[66] [d] B3LYP,[72] Def2-TZVP,[66] but with geometry optimization in the cation doublet state, spin unrestricted option.[65] [e] Values practically pairwise equivalent for symmetry reasons.

Table 3 ORCA-DFT results for isotropic ^{1}H hyperfine coupling constants a_H^{th} in cation radicals of *T1*-**1** (Möbius) and *T2*-**1** (Hückel), respectively. Meaning of suffixes same as in Table 2

		a_H^{th}/MHz	
Case[a]	Structure[b]	H(N_{34})	H(N_{38})
3[c]	*T1*-**1**	−3.63	−4.58
	T2-**1**	−4.22	−4.23[e]
5[d]	*T1*-**1**	−2.56	−5.13

[a] Different program settings (functional, basis-set, *etc.*). [b] Initial geometries from optimized X-ray structures.[20] [c] B3LYP,[72] Def2-TZVP.[66] [d] B3LYP,[72] Def2-TZVP,[66] but with geometry optimization in the cation doublet state, spin unrestricted option.[65] [e] Values practically pairwise equivalent for symmetry reasons.

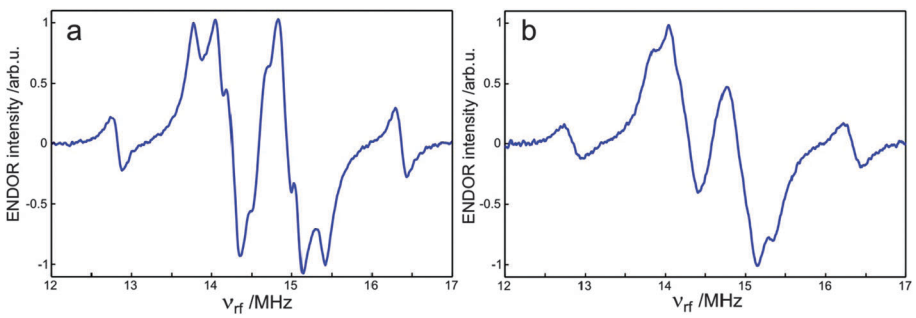

Fig. 2 (a) Experimental ^{1}H-ENDOR-spectrum of the cation radical of *T1*-**1** in CH_2Cl_2 at 190 K. (b) Experimental ^{1}H-ENDOR-spectrum of the cation radical of *T2*-**1** in CH_2Cl_2 at 300 K. The cw ENDOR spectra are shown in the usual first-derivative representation with respect to the rf frequency, ν_{rf}. After applying low-pass filtering, both ENDOR spectra in (a) and (b) have been corrected for base line drifts and amplitude variations due to hyperfine enhancement of the applied rf field.[56]

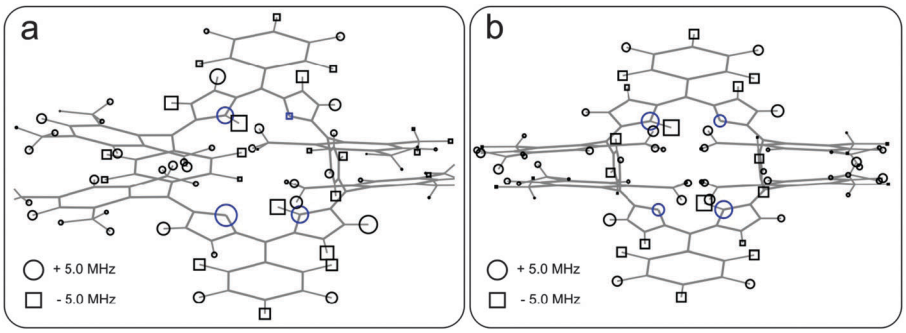

Fig. 3 Theoretical hyperfine couplings in the *T1*-**1** (a) and *T2*-**1** (b) open-shell cation electronic states (as specified in each figure). Black and blue circles or squares refer to protons and nitrogens, respectively. The hyperfine couplings are proportional to the areas of the respective squares ($a < 0$) and circles ($a > 0$).

and proton isotropic hfc-values appear practically pairwise equivalent in *T2*-**1**. The four nitrogen couplings in the *T1*-**1** structure appear rather scrambled over nearly the same frequency range as in *T2*-**1**. This fact explains some of the problems encountered in the analysis of the ENDOR-spectrum of *T1*-**1** due to partial overcrowding of certain spectral regions. For this reason, additional computational approaches, *e.g.*, Cases 4 to 7 presented in Tables S1 and S2 in ESI,† were chosen for *T1*-**1** in the attempt to get a closer agreement between experimental and theoretical *a*-values.

The comparatively best result for *T1*-**1** (Möbius) was achieved in Case 5 by using the functional/basis-set B3LYP/Def2-TZVP in conjunction with a geometry optimization procedure in the radical cation open-shell doublet state. However, there remains a maximum discrepancy of 0.7 MHz between theoretical and experimental results, which is still quite satisfying in view of the complexity of the electronic structure with its 419 valence electrons. As shown in Fig. 4, the changes between the optimized neutral singlet and the optimized charged doublet state structures of *T1*-**1** turned out to be small (<0.03 Å).

As potential candidates for structural changes, we considered the N–H bond lengths as well as various C–C and C–N bond lengths in the macrocycle (see Fig. 4). Changes in the attached mesityl and phenyl rings (see Scheme 1) turned out to be negligibly small (<0.001 Å) and are therefore not displayed. The largest changes (≈ 0.03 Å) occur in the C–C bonds between the macrocycle and the benzene ring having its plane positioned vertically to the mean molecular plane.

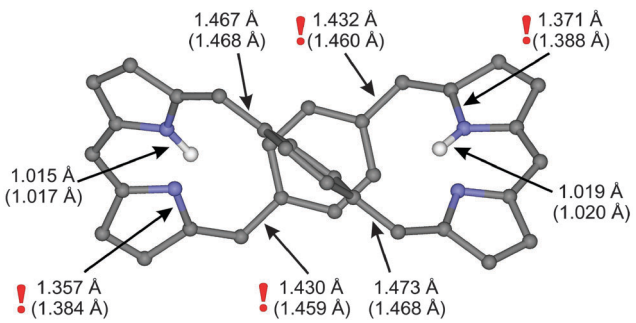

Fig. 4 Specific structural changes between the geometry optimized doublet and singlet states (in brackets) of T1-**1** (Möbius topology). For the sake of clarity, all mesityl- and phenyl groups (see Scheme 1) as well as all hydrogen atoms have been omitted, except those belonging to the two N–H bonds. The largest changes are marked with a red exclamation mark. For more details, see text.

Despite the smallness of all these geometrical changes, the effects on particular hfc's are quite significant (compare Cases 3 and 5 for *T1*-**1** in Tables 2 and 3). This demonstrates the strong dependence of the various local isotropic hyperfine interactions on the large-scale (global) features of the molecular orbital (HOMO) carrying the unpaired electron.

A potential problem associated with any quantum chemical calculation on porphyrinoid molecules like compound **1** is the choice of the actually observed tautomers. At the free-base level studied in this work, there are two possible tautomers for the *T2* structure (each of C_2 symmetry) and three for the *T1* structure (two C_2-symmetric and one with C_1 symmetry).[9] Energies for all tautomer structures *in vacuo* are given in ref. 9 (Table S5, ESI†). The energy difference between the tautomers of *T2* is small (0.26 kcal mol^{-1}), but for *T1* the spread of energies is larger. In particular, the structure of *T1* with C_1 symmetry that originally was given in ref. 10 and used in the present work's calculations, is not the lowest energy structure according to the DFT calculations.[9] There exists a tautomer with C_2 symmetry that is 0.72 kcal mol^{-1} lower in energy, it is shown in Scheme 1. In the present work, we focus on the radical cations and, hence, in principle, we should consider the energy ordering for the cations rather than that for the neutral species. The ENDOR measurements on the cation radical of *T1* clearly show a C_1 symmetry on the basis of the higher number of ^{14}N hyperfine lines than allowed for a C_2 symmetry. Thus, the energy ordering in the cations turns out to be not identical with that in the neutral singlet-state molecule.

5. Summary and conclusion

The EPR and ENDOR study on radical cations of di-*p*-benzi-[28]hexaphyrin-(1.1.1.1.1.1) presented here allowed to discriminate between topologically different conformers, the Hückel structure *T2*-**1** and the Möbius structure *T1*-**1**. Evidencing the topological switch between the two conformers is not feasible alone by spectroscopic experiments but must be corroborated by quantum chemical calculations of the spin density distributions. For this purpose, we applied state-of-the-art DFT theory using different

refinements of functionals and basis sets supplied by the ORCA program package. The hyperfine-coupling results of these various refinements are collected in Tables S1 and S2 of the ESI† (and partly in the main text).

As the main result, it turned out that the open-shell cation-radical system, regardless of its number of π-electrons, exhibits the ability to change between Hückel and Möbius topologies, similar to what is known for the closed-shell system. This result is corroborated by extended DFT calculations searching for total-energy minima of the electronic structure on twisting the molecular framework. The DFT calculations indicate, however, that there is only a small energy gap between Hückel and Möbius conformations in [28]hexaphyrins. Apparently, Hückel and Möbius structures coexist as an equilibrium in compound **1** which depends on temperature and is shifted at low temperature towards the Möbius conformer.[20]

In this context, and as an outlook, additional EPR and ENDOR studies on the relationship between Hückel–Möbius aromaticity and topological properties of expanded porphyrins in their open-shell electronic configurations constitute an important extension of the present research. They are anticipated to provide further insight into the understanding of the electronic and magnetic characteristics of Möbius-band aromatic molecules. Both ground-state radical anions ($S = 1/2$) and photoexcited triplet states ($S = 1$) of hexaphyrin **1** are envisaged as suitable candidates of such studies, and first experiments are in progress in our laboratories.

Acknowledgements

We acknowledge with gratitude the scientific and personal interactions with Prof. Seigo Yamauchi, our late colleague at Tohoku University in Sendai. He had told us, at an EPR meeting of the MPI in Mülheim (Ruhr) in June 2011, that he was just performing X-band EPR studies on the photoexcited triplet state of a molecule with Möbius topology synthesized in the Kyoto group. About a year later we had to realize with great sadness that Seigo Yamauchi could not finish this work because he had unexpectedly passed away on September 26, 2012, at the age of only 64. We express our thanks to Rolf Trinoga, IT Group Leader at the MPI for Chemical Energy Conversion (CEC) in Mülheim, for his kind assistance in our ORCA-DFT calculations on the CEC Hermes computer cluster. K. M., M. P., G. K., C. L., A. S. and W. L. gratefully acknowledge support by the Max Planck Society and the Free University Berlin. This work is supported by the Cluster of Excellence RESOLV (EXC 1069) funded by the Deutsche Forschungsgemeinschaft. The work at the University of Wrocław was supported by the Polish National Science Centre. Grant Numbers: 2012/04/A/ST5/00593, UMO-2011/01/N/ST5/02557. We thank the referees for helpful comments.

References

1 S. M. Rosen, *Science, paradox, and the Moebius principle: the evolution of a ''transcultural'' approach to wholeness*, State University of New York Press, Albany, 1994.
2 R. Herges, *Naturwiss. Rundsch.*, 2005, **58**, 301–310.
3 R. Herges, *Chem. Rev.*, 2006, **106**, 4820–4842.
4 G. R. Schaller and R. Herges, *Chem. Commun.*, 2013, **49**, 1254–1260.
5 A. F. Möbius, *Berichte über die Verhandlungen der Königlich Sächsischen Gesellschaft der Wissenschaften zu Leipzig, Math.-Phys. Classe*, 1865, vol. 11, pp. 31–68.
6 J. B. Listing, *Abhandlungen der Königlichen Gesellschaft der Wissenschaften zu Göttingen, Math. Classe*, 1861, vol. 10, pp. 97–182.
7 C. A. Pickover, *The Möbius Strip: Dr. August Möbius's Marvellous Band in Mathematics, Games, Literature, Art, Technology, and Cosmology*, Basic Books, New York, 2006.
8 E. Heilbronner, *Tetrahedron Lett.*, 1964, 1923–1928.
9 M. Stępień, B. Szyszko and L. Latos-Grażyński, *J. Am. Chem. Soc.*, 2010, **132**, 3140–3152.
10 M. Stępień, N. Sprutta and L. Latos-Grażyński, *Angew. Chem., Int. Ed.*, 2011, **50**, 4288–4340.
11 Y. Tanaka, S. Saito, S. Mori, N. Aratani, H. Shinokubo, N. Shibata, Y. Higuchi, Z. S. Yoon, K. S. Kim, S. B. Noh, J. K. Park, D. Kim and A. Osuka, *Angew. Chem., Int. Ed.*, 2008, **47**, 681–684.
12 J. M. Lim, J.-Y. Shin, Y. Tanaka, S. Saito, A. Osuka and D. Kim, *J. Am. Chem. Soc.*, 2010, **132**, 3105–3114.
13 C.-W. Chang, M. Liu, S. Nam, S. Zhang, Y. Liu, G. Bartal and X. Zhang, *Phys. Rev. Lett.*, 2010, **105**, 235501.
14 E. Hückel, *Z. Phys.*, 1931, **70**, 204–286.
15 E. Hückel, *Z. Phys.*, 1932, **76**, 628–648.
16 E. Hückel, *Grundzüge der Theorie Ungesättiger und aromatischer Verbindungen*, VCH, Berlin, 1938.
17 H. E. Zimmerman, *J. Am. Chem. Soc.*, 1966, **88**, 1564–1565.
18 C. Castro, C. M. Isborn, W. L. Karney, M. Mauksch and P. V. Schleyer, *Org. Lett.*, 2002, **4**, 3431–3434.
19 H. S. Rzepa, *Chem. Rev.*, 2005, **105**, 3697–3715.
20 M. Stępień, L. Latos-Grażyński, N. Sprutta, P. Chwalisz and L. Szterenberg, *Angew. Chem., Int. Ed.*, 2007, **46**, 7869–7873.
21 G. Bucher, S. Grimme, R. Huenerbein, A. A. Auer, E. Mucke, F. Koehler, J. Siegwarth and R. Herges, *Angew. Chem., Int. Ed.*, 2009, **48**, 9971–9974.
22 E.-K. Mucke, F. Koehler and R. Herges, *Org. Lett.*, 2010, **12**, 1708–1711.
23 T. Kawase and M. Oda, *Angew. Chem., Int. Ed.*, 2004, **43**, 4396–4398.
24 Z. S. Yoon, A. Osuka and D. Kim, *Nat. Chem.*, 2009, **1**, 113–122.
25 D. Ajami, K. Hess, F. Koehler, C. Nather, O. Oeckler, A. Simon, C. Yamamoto, Y. Okamoto and R. Herges, *Chem. – Eur. J.*, 2006, **12**, 5434–5445.
26 D. Ajami, O. Oeckler, A. Simon and R. Herges, *Nature*, 2003, **426**, 819–821.
27 M. Stępień, B. Szyszko and L. Latos-Grażyński, *Org. Lett.*, 2009, **11**, 3930–3933.
28 B. Szyszko, N. Sprutta, P. Chwalisz, M. Stępień and L. Latos-Grażyński, *Chem. – Eur. J.*, 2014, **20**, 1985–1997.
29 Y. Tanaka, S. Saito, S. Mori, N. Aratani, H. Shinokubo, N. Shibata, Y. Higuchi, Z. S. Yoon, K. S. Kim, S. B. Noh, J. K. Park, D. Kim and A. Osuka, *Angew. Chem., Int. Ed.*, 2008, **47**, 681–684.

30 J.-Y. Shin, K. S. Kim, M.-C. Yoon, J. M. Lim, Z. S. Yoon, A. Osuka and D. Kim, *Chem. Soc. Rev.*, 2010, **39**, 2751–2767.
31 E. Pacholska-Dudziak, J. Skonieczny, M. Pawlicki, L. Szterenberg, Z. Ciunik and L. Latos-Graynski, *J. Am. Chem. Soc.*, 2008, **130**, 6182–6195.
32 J. K. Park, Z. S. Yoon, M.-C. Yoon, K. S. Kim, S. Mori, J.-Y. Shin, A. Osuka and D. Kim, *J. Am. Chem. Soc.*, 2008, **130**, 1824–1825.
33 J. Sankar, S. Mori, S. Saito, H. Rath, M. Suzuki, Y. Inokuma, H. Shinokubo, K. S. Kim, Z. S. Yoon, J.-Y. Shin, J. M. Lim, Y. Matsuzaki, O. Matsushita, A. Muranaka, N. Kobayashi, D. Kim and A. Osuka, *J. Am. Chem. Soc.*, 2008, **130**, 13568–13579.
34 S. Tokuji, J.-Y. Shin, K. S. Kim, J. M. Lim, K. Youfu, S. Saito, D. Kim and A. Osuka, *J. Am. Chem. Soc.*, 2009, **131**, 7240–7241.
35 K. S. Kim, Z. S. Yoon, A. B. Ricks, J.-Y. Shin, S. Mori, J. Sankar, S. Saito, Y. M. Jung, M. R. Wasielewski, A. Osuka and D. Kim, *J. Phys. Chem. A*, 2009, **113**, 4498–4506.
36 S. Saito, J.-Y. Shin, J. M. Lim, K. S. Kim, D. Kim and A. Osuka, *Angew. Chem., Int. Ed.*, 2008, **47**, 9657–9660.
37 T. Koide, K. Youfu, S. Saito and A. Osuka, *Chem. Commun.*, 2009, 6047–6049.
38 T. Higashino, M. Inoue and A. Osuka, *J. Org. Chem.*, 2010, **75**, 7958–7961.
39 T. Higashino, J. M. Lim, T. Miura, S. Saito, J.-Y. Shin, D. Kim and A. Osuka, *Angew. Chem., Int. Ed.*, 2010, **49**, 4950–4954.
40 T. Higashino, B. S. Lee, J. M. Lim, D. Kim and A. Osuka, *Angew. Chem., Int. Ed.*, 2012, **51**, 13105–13108.
41 M. Inoue, K. S. Kim, M. Suzuki, J. M. Lim, J.-Y. Shin, D. Kim and A. Osuka, *Angew. Chem., Int. Ed.*, 2009, **48**, 6687–6690.
42 M. Inoue and A. Osuka, *Angew. Chem., Int. Ed.*, 2010, **49**, 9488–9491.
43 M. Inoue, T. Yoneda, K. Youfu, N. Aratani and A. Osuka, *Chem. – Eur. J.*, 2011, **17**, 9028–9031.
44 A. Osuka and S. Saito, *Chem. Commun.*, 2011, **47**, 4330–4339.
45 H. Rath, S. Tokuji, N. Aratani, K. Furukawa, J. M. Lim, D. Kim, H. Shinokubo and A. Osuka, *Angew. Chem., Int. Ed.*, 2010, **49**, 1489–1491.
46 S. Saito and A. Osuka, *Angew. Chem., Int. Ed.*, 2011, **50**, 4342–4373.
47 T. Tanaka, T. Sugita, S. Tokuji, S. Saito and A. Osuka, *Angew. Chem., Int. Ed.*, 2010, **49**, 6619–6621.
48 T. Tanaka and A. Osuka, *Chem. – Eur. J.*, 2012, **18**, 7036–7040.
49 M.-C. Yoon, P. Kim, H. Yoo, S. Shimizu, T. Koide, S. Tokuji, S. Saito, A. Osuka and D. Kim, *J. Phys. Chem. B*, 2011, **115**, 14928–14937.
50 J. S. Sessler and S. J. Weghorn, *Expanded, Contracted, and Isomeric Porphyrins*, Elsevier, Amsterdam, 1997.
51 K. Berlin and E. Breitmaier, *Angew. Chem., Int. Ed.*, 1994, **33**, 1246–1247.
52 M. Stępień and L. Latos-Grażyński, *Chem. – Eur. J.*, 2001, **7**, 5113–5117.
53 M. Stępień and L. Latos-Grażyński, *J. Am. Chem. Soc.*, 2002, **124**, 3838–3839.
54 M. Stępień and L. L. Grazynski, *Acc. Chem. Res.*, 2005, **38**, 88–98.
55 B. Szyszko, L. Latos-Grażyński and L. Szterenberg, *Angew. Chem., Int. Ed.*, 2011, **50**, 6587–6591.
56 K. Möbius, M. Plato and W. Lubitz, *Phys. Rep.*, 1982, **87**, 171–208.
57 H. Käss, J. Rautter, W. Zweygart, A. Struck, H. Scheer and W. Lubitz, *J. Phys. Chem.*, 1994, **98**, 354–363.
58 W. Zweygart, R. Thanner and W. Lubitz, *J. Magn. Reson.*, 1994, **109**, 172–176.
59 K. Möbius and R. Biehl, in *Mulitiple Electron Resonance Spectroscopy*, ed. M. M. Dorio and J. H. Freed, Plenum, New York, 1979, pp. 475–507.
60 W. Lubitz, R. A. Isaacson, E. C. Abresch and G. Feher, *Proc. Natl. Acad. Sci. U. S. A.*, 1984, **81**, 7792–7796.
61 A. Carrington and A. D. McLachlan, *Introduction to Magnetic Resonance*, Harper and Row, New York, 1969.
62 R. G. Parr and W. Yang, *Density-Functional Theory of Atoms and Molecules*, Oxford University Press, Oxford, 1989.
63 W. Koch and M. C. Holthausen, *A Chemist's Guide to Density Functional Theory*, Wiley-VCH, Weinheim, 2000.
64 F. Neese, *Wiley Interdiscip. Rev.: Comput. Mol. Sci.*, 2012, **2**, 73–78.
65 R. Ditchfield, W. J. Hehre and J. A. Pople, *J. Chem. Phys.*, 1971, **54**, 724–728.
66 F. Weigend and R. Ahlrichs, *Phys. Chem. Chem. Phys.*, 2005, **7**, 3297–3305.
67 A. Klamt and G. Schüürmann, *J. Chem. Soc., Perkin Trans. 2*, 1993, 799–805.
68 T. O'Have, A Pragmatic Introduction to Signal Processing, http://terpconnect.umd.edu/~toh/spectrum/TOC.html.
69 M. Huber, H. Kurreck, B. von Maltzan, M. Plato and K. Möbius, *J. Chem. Soc., Faraday Trans.*, 1990, **86**, 1087–1094.
70 M. N. Khan, C. Palivan, F. Barbosa, J. Amaudrut and G. Gescheidt, *J. Chem. Soc., Perkin Trans. 2*, 2001, 1522–1526.
71 N. M. Atherton, *Principles of Electron Spin Resonance*, Ellis Horwood, New York, 1993.
72 A. D. Becke, *J. Chem. Phys.*, 1993, **98**, 5648–5652.

